Electronic stopping cross sections for protons in Al₂O₃:
an experimental and theoretical study

M. Behar, R.C. Fadanelli, L.C.C.M. Nagamine, E.D. Cantero , G.H. Lantschner, J.C. Eckardt, N.R. Arista ,
R. Garcia-Molina and I. Abril

**THE EUROPEAN
PHYSICAL JOURNAL D**

Regular Article

Electronic stopping cross sections for protons in Al₂O₃: an experimental and theoretical study

M. Behar[1], R.C. Fadanelli[1], L.C.C.M. Nagamine[2], E.D. Cantero[3], G.H. Lantschner[3], J.C. Eckardt[3], N.R. Arista[3], R. Garcia-Molina[4], and I. Abril[5,a]

[1] Instituto de Fisica, Universidade Federal do Rio Grande do Sul, 91501-970 Porto Alegre, Brazil
[2] Instituto de Fisica, Universidade de São Paulo, 05508-090 São Paulo, Brazil
[3] Centro Atómico Bariloche and Instituto Balseiro, Comisión Nacional de Energía Atómica, 8400 San Carlos de Bariloche, Argentina
[4] Departamento de Física – Centro de Investigación en Óptica y Nanofísica, Universidad de Murcia, 30100 Murcia, Spain
[5] Departament de Física Aplicada, Universitat d'Alacant, 03080 Alacant, Spain

Abstract. The electronic stopping cross section (SCS) of Al₂O₃ for proton beams is studied both experimentally and theoretically. The measurements are made for proton energies from 40 keV up to 1 MeV, which cover the maximum stopping region, using two experimental methods, the transmission technique at low energies (∼40–175 keV) and the Rutherford backscattering at high energies (≈190–1000 keV). These new data reveal an increment of 16% in the SCS around the maximum stopping with respect to older measurements. The theoretical study includes electronic stopping power calculations based on the dielectric formalism and on the transport cross section (TCS) model to describe the electron excitations of Al₂O₃. The non-linear TCS calculations of the SCS for valence electrons together with the generalized oscillator strengths (GOS) model for the core electrons compare well with the experimental data in the whole range of energies considered.

1 Introduction

Alumina (Al₂O₃) is an important material broadly used in mechanical, optical, optoelectronics or microelectronic applications due to its excellent chemical resistance, good mechanical strength, high hardness, transparency, high abrasion and corrosion resistance. All these remarkable properties make of Al₂O₃ a typical choice as a matrix/substrate for optical waveguide amplifiers in integrated systems [1], solid state lasers or thin-film devices [2,3]. Also, the electronic properties of Al₂O₃ films allow their use as gate dielectric for field-effect transistors [4], whereas the capability to insert nanocomposites in alumina matrices suggests potential applications in nanoscale memory devices [5].

On the other hand, the study of the energy deposition of energetic ions in matter is a problem of interest for basic and applied research in many areas, such as ion implantation, ion beam analysis and modification of materials, radiation damage, radiation therapy or space research [6–8]. Therefore due to the importance of alumina films, it is desirable to know accurately their stopping power in a wide range of ion energies, since it plays a key role in ion beam analysis experiments.

The stopping power of proton beams in Al₂O₃ was studied since the early sixties [9]. Later on, more results were reported for a wide range of projectile energies [10–13]. Measurements for slow H⁺ projectiles were done by Eder et al. [14] looking for a threshold effect in the velocity dependence of the stopping power, however despite the fact that alumina is a large-band-gap insulator, a linear velocity dependence was found. These authors also claimed that the strong chemical bonds in Al₂O₃ play an important role in the stopping power [14]. A more recent theoretical-experimental study for H⁺, He⁺ and N⁺ projectiles in Al₂O₃ and SiO₂ was made by [15] in order to understand the differences in the stopping behaviour of both targets.

It also calls the attention that the stopping power of Al₂O₃ for H⁺ projectiles predicted by the semi-empirical SRIM code [16], both with and without chemical corrections, does not agree with the previous published data. This fact, together with a significant dispersion among the experimental stopping data [17], has been an incentive to carry out new measurements of the stopping power of Al₂O₃ for H⁺ in a broad range of energies, which includes the maximum stopping region.

We present here an experimental-theoretical study of the stopping power of Al₂O₃ for proton beams. With

[a] e-mail: ias@ua.es

this purpose we have measured the stopping cross section (SCS) on a wide energy range, from 40 keV up to 1 MeV, using two techniques: Rutherford backscattering spectrometry (RBS) and the transmission method, both described in Section 2. Theoretical calculations of the SCS based on the linear dielectric formalism and on the non-linear transport-cross-section model are presented in Section 3. In Section 4, we show our new experimental data for the stopping power and a comparison with the theoretical calculations. Finally, the conclusions of this work are outlined.

2 Experimental methods

For the determination of the stopping power of the Al_2O_3 target for a proton beam we have used two techniques: the RBS for the higher energies, and the foil transmission method for the lower ones.

For the RBS experiments, the Al_2O_3 films were prepared by radio frequency magnetron sputtering using a commercial target and O_2/Ar mixture as a sputtering gas. The sample had a nominal purity of 99.99%. Films of thicknesses 43, 72 and 117 nm were deposited on a gold film which was previously evaporated over a silicon substrate. We have followed this procedure because the fact that the Si signal of the substrate overlaps the Al_2O_3 signal. Therefore, with the present substrate/films structure ($Si/Au/Al_2O_3$), instead of determining the energy loss that the H ions suffer in the Al_2O_3 films by using the signal corresponding to the projectiles backscattered in the Al or O atoms, we have developed the method described below.

We used as a marker the high energy edge of the Au signal, which corresponds to projectiles backscattered in the outermost layer of Au. Those projectiles, in addition to the elastic energy loss in the backscattering event, also lose energy in the inward and outward paths of the Al_2O_3 film. The energy loss in the alumina film was determined by performing a comparison with the energy of ions backscattered at an Au surface, as illustrated in Figure 1. The thickness of the Al_2O_3 films was determined by using the energy loss of a He^+ beam at 3 MeV, and normalizing with the predicted stopping power of the SRIM code [16].

The RBS technique was used in the 190–1000 keV energy range. The total energy resolution of the system was 6 keV (FWHM), which is due to the intrinsic straggling in the energy loss and to the Al_2O_3 film thickness inhomogeneities. The ion beam was provided by the 500 kV ion implanter and the 3 MV Tandetron accelerator of the Instituto de Física of the Universidade Federal do Rio Grande do Sul.

The samples were mounted on a four axis goniometer and the detector was fixed at 120° with respect to the incident ion beam. For each incident energy, four RBS spectra were recorded at 0°, 20°, 40° and 60° between the sample and the ion beam direction. The selection of the films was done according to the beam energy. In some cases, for a given energy, two different films were used and the obtained results were consistent.
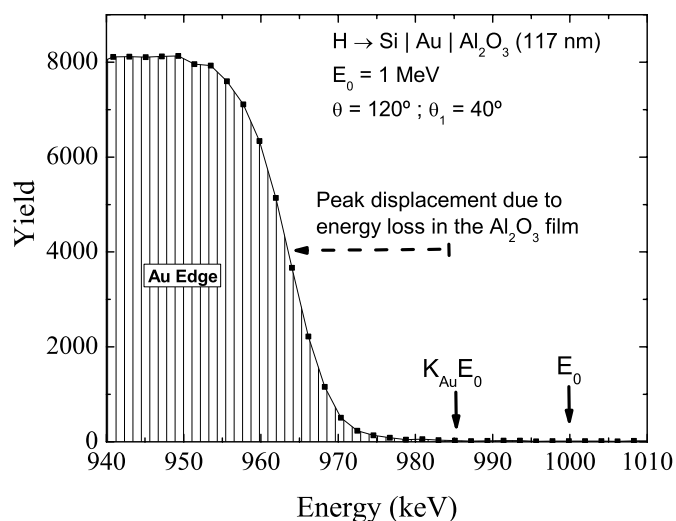
Fig. 1. Rutherford backscattering spectrum taken with a H^+ ion beam at 1 MeV. The angle of the incident ion beam direction with the sample normal is 40°, and the angle with the detector is 120°. This energy region corresponds to projectiles that have reached the detector after a backscattering collision with an Au atom. The high energy edge of the Au peak is displaced toward lower energies with respect to a backscattering event occurring at an Au surface due to the energy loss in the Al_2O_3 film.

For the data analysis we used the mean-energy approximation, which in the present case is more suitable than the surface one [18]. In the mean-energy approximation, for a fixed beam-detector geometry two measurements are necessary at different beam-sample geometries in order to obtain the stopping power for the inward and outward paths along the sample. Usually we had four different geometries for the same energy. Consequently we have a set of equations from which we can determine the corresponding stopping powers with very good precision. Proceeding in this way we have obtained the H^+ stopping power from the RBS measurements.

The energy loss determinations for H^+ projectiles in Al_2O_3 with energies between 40 and 175 keV were done at the Atomic Collisions Laboratory of the Centro Atómico Bariloche, employing the transmission method. The ion beams were generated by an electrostatic accelerator with an radio frequency ion source followed by focusing and mass selection stages. The Al_2O_3 foils were mounted on a movable holder to allow energy measurements of the direct beam and the beam transmitted through the target. The energy analysis was performed by an electrostatic analyzer with 0.3% FWHM resolution positioned in the forward beam direction. The particles were detected by an electron multiplier followed by conventional pulse counting electronics. Spectra were recorded by a multichannel scaler with channels switched synchronously with the energy-analyzer plate potential.

Target charging up was avoided by introducing a low-energy electron shower in the target chamber and working with low beam current densities ($\sim 10^{-9}$ A/cm^2). These

low current densities combined with short measuring times of ~2 min per spectrum also avoided foil thickening by the beam.

The self supported foils were made by electron-gun evaporation under clean vacuum conditions on a very smooth plastic substrate which was subsequently dissolved [19]. The mean foil thickness of the Al_2O_3 targets was 33 nm and has been determined by energy-loss measurements and normalization to 200 keV stopping power values from the SRIM code [16]. It should be mentioned that the main source of errors in the determination of the stopping power relies on the thickness film determination.

3 Theoretical models

Since the present study of the energy loss of proton beams in alumina films covers a wide range of projectile energies, which include regions below and over the stopping power maximum, the theoretical description contain two different approaches: the dielectric formulation and the quantum transport cross section model. Detailed reports of these formulations have been given before [20–23], so just a brief summary of each of them will be exposed. Due to the projectile energy range considered in this work, only the electronic energy loss will be considered, neglecting elastic collisions with target nuclei [24].

In the equilibrium regime, the electronic stopping power $S = -\langle dE/dx \rangle$ for a projectile with atomic number Z_1, moving with energy E in a target, is a weighted average of the stopping powers S_q corresponding to the different charge states q of the projectile resulting from the electron capture and loss processes during its travel through the solid,

$$S = \sum_{q=0}^{Z_1} \phi_q \, S_q. \tag{1}$$

Here ϕ_q is the probability of finding the projectile in a given charge state q at energy E, which depends on the target nature, the projectile and its energy. The charge-state fractions ϕ_q at equilibrium are obtained from a parameterization to experimental data [25], which uses Bragg's additivity rule for compound targets. The summation in equation (1) extends over all possible charge states q of the projectile.

As indicated before, two different approaches to evaluate the inelastic energy loss of energetic projectiles in solids are considered. The dielectric formalism based on perturbative approximations for dense media, which can be applied to swift projectiles, and the non-linear transport cross section (TCS) model, which is used to evaluate the electron valence contribution to the stopping power on a wide range of energies. Here we give a brief description of each of these methods.

3.1 Dielectric model

The dielectric formulation is a standard treatment of the interaction of charged particles with condensed media

based on first order perturbation theory [26], where the dielectric response function of the target $\varepsilon(k, \omega)$ provides a description of the dynamical potential induced by swift ions in solids. As a result of this interaction, the incoming projectile, with kinetic energy E, mass M_1 and charge state q, will lose energy in the process to induce electronic excitations in the target. With this formalism the stopping power is given by

$$S_q = \frac{M_1 e^2}{\pi E} \int_0^\infty \frac{dk}{k} \rho_q^2(k) \int_0^{k\sqrt{2E/M_1}} d\omega \, \omega \text{Im} \left[\frac{-1}{\varepsilon(k, \omega)} \right], \tag{2}$$

where $\hbar k$ and $\hbar \omega$ are, respectively, the transferred momentum and energy from the projectile to the target electrons, $\text{Im} \left[-1/\varepsilon(k, \omega) \right]$ is the energy loss function (ELF) of the target, which is the main magnitude to characterize the response of the target to an external electromagnetic perturbation. ρ_q is the Fourier transform of the projectile charge-density for the charge state q, calculated here using the statistical Brandt-Kitagawa model [27][1].

We describe the ELF of the target by the MELF-GOS model (Mermin-Energy-Loss-Function-Generalized-Oscillator-Strengths) [20,21,29], where the target electron excitations are split into two parts, the inner excitations related to the inner-shell electrons, and the outer excitations corresponding to the weakly-bound electrons. As the inner-shell electrons have relatively large binding energies and negligible collective effects, they are described using a single-atom model through the Generalized Oscillator Strengths (GOS) in the hydrogenic approach [30]. On the other hand, the outer electron excitations are modelled by a linear combination of Mermin-type ELF [31], which is constructed by a fitting to available experimental ELF values at the optical limit ($k = 0$). The ELF obtained in this way must also satisfy the f-sum rule for all values of the transferred momentum. With this approach a complete representation of the energy and momentum dependence of the ELF is automatically obtained due to the analytical properties of the Mermin-ELF and the GOS. Note that this method incorporates realistically the dielectric properties of the target, such as individual or collective excitations, aggregation and chemical effects of condensed matter, as well as the finite plasmon lifetime of the Mermin dielectric function, since it is based on optical ELF experimental data.

There are two sets of experimental data for the ELF of Al_2O_3 at the optical limit [32,33], obtained from vacuum ultraviolet spectroscopy and from electron energy-loss spectroscopy, and although both measurements present a well defined peak at ~25 eV, there are sizeable differences in their absolute values [34]. The dielectric properties of Al_2O_3 are described by the MELF-GOS methodology, where the K-shell electrons of Al and O are treated as inner-electrons through their GOS, since they show negligible collective effects due to their large binding energies; the rest of the electrons are considered as outer electrons and treated by the MELF model, as reported previously [35]. We applied the MELF-GOS methodology to

---

[1] Corrections to the BK model appear in [28].

both sets of optical experimental ELF data of alumina in order to calculate the proton stopping power as given by equations (1) and (2).

3.2 Transport cross section model

The transport cross section (TCS) formalism is a non-perturbative quantum method to calculate the scattering of electrons in a screened potential and obtain the valence electron contribution to the electronic stopping power [36]. This approach is based on numerical integrations of the Schrödinger equation for a screened potential representing the interaction with the target electrons of the ion, having a charge state q and moving with velocity v; from these calculations one obtains the values of the phase shifts $\delta_l(v_r, v)$ as a function of the relative electron-ion velocity v_r, which are then used to calculate the transport cross section $\sigma_{tr}(v_r, v)$ by the equation

$$\sigma_{tr}(v_r, v) = \frac{4\pi}{v_r^2} \sum_{l=0}^{\infty} (l+1) \sin^2[\delta_l(v_r, v) - \delta_{l+1}(v_r, v)]. \quad (3)$$

Then, to obtain the mean energy transfer to the medium one must perform an integration over the distribution of the electron speeds v_e, using the following relation [37] to obtain the valence electron stopping power,

$$S_{q, \text{valence}} = \frac{1}{4\pi^2 v^2} \int_0^{v_F} v_e dv_e$$
$$\times \int_{|v-v_e|}^{|v+v_e|} dv_r v_r^4 \sigma_{tr}(v_r, v) \left[1 + \frac{v^2 - v_e^2}{v_r^2}\right] \quad (4)$$

where v_F is the Fermi velocity of the target valence electrons. The set of calculations must be repeated for each ion speed of interest. This approach has the advantage of providing a fully non-perturbative method to calculate the stopping power, and is also called a *non-linear* approach, since it applies to all orders in the interaction. More details on this method may be found in several previous publications [22,23,36,38].

The stopping power for a projectile with a charge state q can be calculated separately as due to the contribution of valence electrons plus the inner-shell electron excitations,

$$S_q = S_{q, \text{valence}} + S_{q, \text{inner}}. \quad (5)$$

Here the valence electrons contribution $S_{q, \text{valence}}$ is evaluated from the non-linear transport cross section model, equation (4), whereas the inner-shell electrons part $S_{q, \text{inner}}$ is calculated with the atomic collisional model represented by the GOS in the hydrogenic approach.

In order to represent the interaction of hydrogen beams with Al_2O_3 targets, the calculations of $S_{q, \text{valence}}$ were made for the two relevant ion charges: protons and neutral hydrogen, and finally the results were averaged considering the equilibrium charge state values for each ion energy (see Eq. (1)). The valence electrons of Al_2O_3
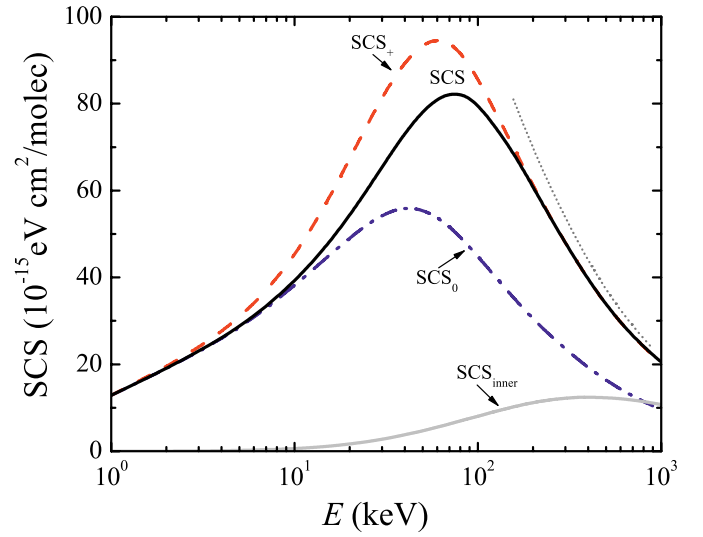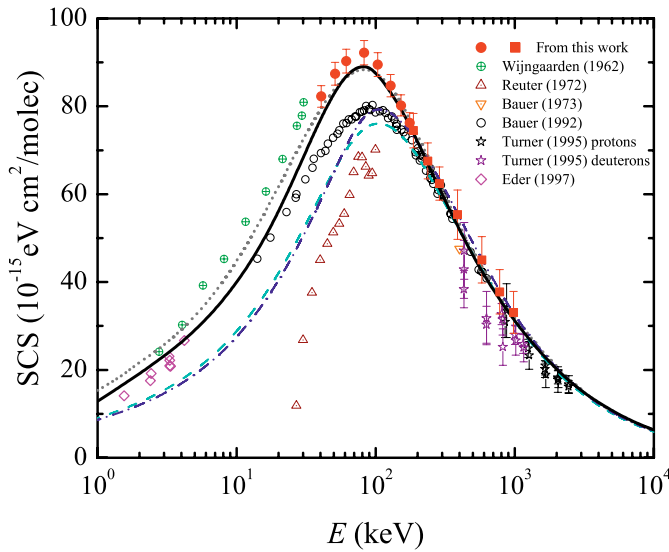

Fig. 2. (Color online) Valence stopping cross section (SCS) of Al_2O_3 as a function of the incident energy of a proton beam, calculated by the non-lineal transport cross section model for $r_s = 1.5$ a.u. (due to valence electrons). The red dashed line (SCS$_+$) represents the results for H$^+$, the blue dash-dotted line (SCS$_0$) corresponds to H^0, whereas the black solid line is the total valence SCS, obtained from the previous SCS weighted with the equilibrium charge fractions (Eq. (1)). The grey solid line (SCS$_{\text{inner}}$) represents the contribution to the SCS due to the inner-shell electrons, obtained with the GOS model. The grey dotted line represents the Bethe SCS for an electron gas with $r_s = 1.5$ a.u.

were described as a Fermi gas characterized by an one-electron radius, $r_s = 1.5$ a.u., which corresponds to the value of the experimental plasma frequency of alumina ($\sim$25 eV) [32,33].

The stopping cross section, SCS, is defined as SCS $= (1/\rho)S$, where ρ is the target molecular density. In Figure 2 we show the results for the stopping cross section in Al_2O_3. Calculations are shown for the valence SCS obtained with the TSC model for H$^+$ (SCS$_+$, red dashed line) and H^0 (SCS$_0$, blue dash-dotted line), as well as the total SCS (black solid line), provided by a proper weighting with the corresponding equilibrium charge state fractions, according to equation (1). At projectile energies greater that 150 keV only the H$^+$ component contributes to the SCS because above this energy the fraction of H^0 is negligible.

In this approach, we consider as inner-shell electrons of Al_2O_3 those corresponding to the K-shell of O and the K- and L-shells of Al, which were represented by the GOS model to obtain their contribution to the stopping power, equation (5). In Figure 2, the inner-shell contribution to the stopping cross section, SCS$_{\text{inner}}$, is depicted by a grey solid line. The contribution of SCS$_{\text{inner}}$ to the total stopping cross section SCS (due to valence plus inner shells), is SCS$_{\text{inner}}$ $\sim$9% SCS at 100 keV, SCS$_{\text{inner}}$ $\sim$27% SCS at 500 keV, and SCS$_{\text{inner}}$ $\sim$35% SCS at 1000 keV. We conclude that at low proton energies the interaction between the projectile and the valence electrons is the

Fig. 3. (Color online) Stopping cross section (SCS) of Al_2O_3 measured in this work for a proton beam as a function of the incident energy are represented by red circles and squares. Other symbols correspond to experimental data available in the literature [9–14]. Black solid line corresponds to the SCS from the non-lineal transport cross-section model for the valence electrons together with the inner electron excitations from the GOS model. Blue dash-dotted line and cyan dashed line are the results from the dielectric formalism with the MELF-GOS model using the optical experimental ELF from [33] and [32], respectively. The result obtained by the semiempirical SRIM code [16] is depicted by a grey dotted line.

dominant mechanism, while the inner-shell contribution becomes significant for energies above 100 keV.

Finally, we also show in Figure 2, with a grey dotted line, the SCS obtained from the Bethe formula for a free electron gas [39] with $r_s = 1.5$ a.u., which is valid at high projectile energies, and therefore coincides with the more detailed TCS calculation.

4 Results and summary

In Figure 3 we show our present experimental results for the stopping power of Al_2O_3 targets for proton beams, together with previous published results and the estimations from theoretical models. We have depicted with red circle and square symbols the experimental stopping cross section (SCS) from 40 keV to 1000 keV proton energies, which covers the region around the maximum stopping, which is around 80 keV. It is worth mentioning that the experimental data obtained from the two different laboratories, using different techniques: transmission (red circles) and RBS (red squares) agree very well at intermediate energies. We compare our results with other available experimental stopping cross sections [9–14], which cover low, intermediate and high proton energies. At energies higher than 200 keV, our experimental data agree with most of the previous measurements within the error bars, however at the maximum of the stopping power our data

are about 16% larger than the preceding data from [12]. It should be stated that all the previous works were done using the transmission technique, while in the present case for energies higher than 200 keV for the first time was used the RBS one. Moreover our experimental data agree well with the present theoretical calculations as well with the semi-empirical SRIM calculations.

We also show in Figure 3 the results of the SCS calculations from the dielectric formalism with the MELF-GOS model to describe the energy-loss spectrum of Al_2O_3 and using two different sources of experimental ELF. The blue dash-dotted line corresponds to the SCS results obtained by fitting the ELF to the experimental optical data from French et al. [33] whereas the cyan dashed line shows the corresponding results when the ELF is fitted to the Hagemman et al. data [32]. In both cases, the calculated SCS is rather similar, although differ in ~5% at the maximum stopping energy, and agree well at proton energies larger than 200 keV. At lower energies these theoretical values underestimate the present experimental data, indicating that non-linear effects start to be important. The MELF-GOS methodology also provides the mean excitation energy, I, which is a useful parameter in the Bethe equation applicable at high energies [24]; using this analysis we obtain $I = 134$ eV, from the French et al. ELF [33] and $I = 146$ eV, from the Hagemann et al. ELF [32].

Finally, the total SCS of Al_2O_3 for protons was obtained as the sum of two contributions: (i) the contribution of valence electrons, calculated with the transport cross section (TCS) formalism; and (ii) the inner-shell contribution, obtained using the GOS method. The result is depicted in Figure 3 by a black solid line. We find these calculations to be in satisfactory agreement with our experimental data on the whole range of energies considered, including the maximum of the stopping power. At low energies, where non-linear effects must be considered, the results of the transport cross section model show a fair agreement with the experimental data from [14], whereas at high energies they converge to the results obtained with the dielectric formalism. For comparison purposes, we have also plotted in Figure 3, as a grey dotted line, the semiempirical predictions of the SRIM code [16], which agree rather well with the new SCS measurements presented in this work.

In summary, the stopping cross section of Al_2O_3 for protons in a wide energy range has been investigated using a combination of different theoretical and experimental methods. Stopping experiments using transmission and RBS techniques have been reported for energies from 40 keV to 1 MeV. In the region around the stopping power maximum (~80 keV) the present experimental results, well reproduced by the theory, are ~16% larger than the previous ones [12]. Calculations based on the linear dielectric formalism and the non-linear transport cross section model have been presented. The combination of the TCS model (to evaluate the contribution of valence electrons) with the atomic GOS model (to evaluate the contribution of inner-shell electrons) yields results that agree

with the experimental data on the wide range of energies here explored.

References

1. M.J. de Castro, A. Suárez-García, R. Serna, C.N. Afonso, J.G. López, Opt. Mater. **29**, 539 (2007)
2. B. Handke, J.B. Simonsen, M. Bech, Z. Li, P.J. Møller, Surf. Sci. **600**, 5123 (2006)
3. T. Murakami, J.H. Ouyang, S. Sasaki, K. Umeda, Y. Yoneyama, Tribol. Int. **40**, 246 (2007)
4. K. Vanbesien, P. De Visschere, P.F. Smet, D. Poelman, Thin Solid Films **514**, 323 (2006)
5. Y. Li, S. Zhang, Y. Liu, T.P. Chen, T. Sritharan, C. Xu, J. Nanosci. Nanotech. **9**, 1 (2009)
6. *Materials Science with Ion Beams*, *Topics in Applied Physics*, edited by H. Bernas (Springer, Heidelberg, 2009), Vol. 116
7. D. Emfietzoglou, R. Garcia-Molina, I. Kyriakou, I. Abril, H. Nikjoo, Phys. Med. Biol. **54**, 3451 (2009)
8. J.E. Turner, *Atoms, Radiation and Radiation Protection* (Wiley-VCH, Weinheim, 2007)
9. A. van Wijngaarden, H.E. Duckworth, Can. J. Phys. **40**, 1749 (1962)
10. F.W. Reuter, H.P. Smith Jr., J. Appl. Phys. **43**, 4228 (1972)
11. W. Bauer, R.G. Musket, J. Appl. Phys. **44**, 2606 (1973)
12. P. Bauer, W. Rossler, P. Mertens, Nucl. Instrum. Methods Phys. Res. B **69**, 46 (1992)
13. D.C. Turner, N.F. Mangelson, L.B. Rees, Nucl. Instrum. Methods Phys. Res. B **103**, 28 (1995)
14. K. Eder, D. Semrad, P. Bauer, R. Golser, P. Maier-Komor, F. Aumayr, M. Peñalba, A. Arnau, J.M. Ugalde, P.M. Echenique, Phys. Rev. Lett. **79**, 4112 (1997)
15. M. Peñalba, J.I. Juaristi, E. Zarate, A. Arnau, P. Bauer, Phys. Rev. A **64**, 012902 (2001)
16. J.F. Ziegler, J.P. Biersack, M.D. Ziegler, *SRIM, The Stopping and Range of Ions in Matter* (SRIM Co., Chester, MD, 2008), http://www.srim.org
17. H. Paul, *Experimental Stopping Power Compilation*, http://www.exphys.uni-linz.ac.at/Stopping/
18. W.K. Chu, J.M. Meyer, M.A. Nicolet, *Backscattering Spectrometry* (Academic Press, New York, 1978)
19. A. Valenzuela, J.C. Eckardt, Rev. Sci. Instrum. **42**, 127 (1971)
20. I. Abril, R. Garcia-Molina, C.D. Denton, F.J. Pérez-Pérez, N.R. Arista, Phys. Rev. A **58**, 357 (1998)
21. S. Heredia-Avalos, R. Garcia-Molina, J.M. Fernández-Varea, I. Abril, Phys. Rev. A **72**, 052902 (2005)
22. A.F. Lifschitz, N.R. Arista, Phys. Rev. A **57**, 200 (1998)
23. A.F. Lifschitz, N.R. Arista, Phys. Rev. A **58**, 2168 (1998)
24. P. Sigmund, *Particle Penetration and Radiation Effects, General Aspects and Stopping of Swift Point Charges* (Springer, Berlin, 2006)
25. G. Schiwietz, P.L. Grande, Nucl. Instrum. Methods Phys. Res. B **175**–**177**, 125 (2001)
26. J. Lindhard, K. Dan. Vidensk. Selsk. Mat. Fys. Medd. **28**, (1954)
27. W. Brandt, M. Kitagawa, Phys. Rev. B **25**, 5631 (1982)
28. W. Brandt, Nucl. Instrum. Methods Phys. Res. **194**, 13 (1982)
29. J.C. Moreno-Marín, I. Abril, R. Garcia-Molina, Nucl. Instrum. Methods Phys. Res. B **193**, 30 (2002)
30. R.F. Egerton, *Electron Energy-Loss Spectroscopy in the Electron Microscope* (Plenum Press, New York, 1989)
31. N.D. Mermin, Phys. Rev. B **1**, 2362 (1970)
32. H.J. Hagemann, W. Gudat, C. Kunz, J. Opt. Soc. Am. **65**, 742 (1975)
33. R.H. French, H. Mullejans, D. Jones, J. Am. Ceram. Soc. **81**, 2549 (1998)
34. M. Behar, R.C. Fadanelli, I. Abril, R. Garcia-Molina, L.C.C.M. Nagamine, Eur. Phys. J. D **64**, 297 (2011)
35. I. Abril, R. Garcia-Molina, C.F. Sanz, N.R. Arista, Nucl. Instrum. Methods Phys. Res. B **190**, 89 (2002)
36. N.R. Arista, A.F. Lifschitz, *Advances in Quantum Chemistry, Theory of the Interaction of Swift Ions with Matter*, Part I (Elsevier, Amsterdam, 2004), Vol. 45, p. 47
37. L. de Ferrariis, N.R. Arista, Phys. Rev. A **29**, 2145 (1984)
38. N.R. Arista, Nucl. Instrum. Methods Phys. Res. B **195**, 91 (2002)
39. D. Pines, *Elementary Excitations in Solids* (W.A. Benjamin Inc., New York, 1964)